Published in final edited form as:
Nature. 2016 January 14; 529(7585): 226–230. doi:10.1038/nature16527.

Intestinal epithelial tuft cells regulate type 2 mucosal responses required for expulsion of helminth parasites

François Gerbe[1,2,3], **Emmanuelle Sidot**[1,2,3], **Danielle J. Smyth**[4], **Makoto Ohmoto**[5], **Ichiro Matsumoto**[5], **Valérie Dardalhon**[3,6], **Pierre Cesses**[1,2,3], **Laure Garnier**[1,2,3], **Marco Bruschi**[1,2,3], **Yvonne Harcus**[4], **Naomi Taylor**[3,6], **Rick M. Maizels**[4], **Philippe Jay**[1,2,3,#]

[1]CNRS, UMR-5203, Institut de Génomique Fonctionnelle, Montpellier, F-34094, France

[2]INSERM, U1191, Montpellier, F-34094, France

[3]Université de Montpellier, UMR-5203, Montpellier, F-34000, France

[4]Institute of Immunology and Infection Research, School of Biological Sciences and Centre for Immunity, Infection and Evolution, University of Edinburgh, UK

[5]Monell Chemical Senses Center, 3500 Market Street, Philadelphia, Pennsylvania 19104, U.S.A

[6]Institut de Génétique Moléculaire de Montpellier, UMR5535 ; Université de Montpellier ; Montpellier ; France

Helminth parasitic infections are a major global health and social burden [1]. The host defence against helminths such as *Nippostrongylus brasiliensis* is orchestrated by type 2 cell-mediated immunity [2]. Induction of type 2 cytokines including IL4 and IL13 induce goblet cell hyperplasia with mucus production, ultimately resulting in worm expulsion [3,4]. However, the mechanisms underlying the initiation of type 2 responses remain incompletely understood. Here, we show that tuft cells are responsible for initiating type 2 responses to parasites by a cytokine-mediated cellular relay. Tuft cells are a rare epithelial cell type in the steady-state intestinal epithelium [5] and have a Th2-related gene expression signature [6]. We show that following infection with helminth parasites, tuft cells undergo a rapid and extensive IL4Rα-dependent amplification due to direct differentiation of epithelial crypt progenitor cells. We found that the *Pou2f3* gene is essential for tuft cell specification. *Pou2f3*$^{-/-}$ mice lack intestinal tuft cells and have defective mucosal type 2 responses to helminth infection: goblet cell hyperplasia is abrogated, and worm expulsion is compromised. Notably, IL4Rα signalling is sufficient to induce expansion of the tuft cell lineage, and ectopic stimulation of this signalling cascade obviates the need for tuft cells in the epithelial cell remodelling of the intestine. Moreover, tuft cells secrete IL25, thereby

[#]correspondence to Philippe Jay, Institut de Génomique Fonctionnelle, 141 rue de la Cardonille, 34093 Montpellier, France; philippe.jay@igf.cnrs.fr; +33434359298.

Author contribution: F.G. performed the majority of the experiments. E.S., D.S., V.D. and P.C., contributed to mouse studies, M.O. and I.M. to characterization of the Pou2f3-deficient mouse line, E.S., L.G. and M.B. to organoid experiments, and Y.H. to parasite life cycle experiments. P.J. and F.G. conceived the study. P.J., F.G. and R.M. designed experiments with contributions from V.D. and N.T. P.J. wrote the manuscript with inputs from F.G. and N.T.

Data deposition: not applicable

The authors declare no competing financial interest.

Europe PMC Funders Author Manuscripts

regulating type 2 immune responses. Our data reveal a novel function of intestinal epithelial tuft cells and demonstrate a cellular relay required for initiating mucosal type 2 immunity to helminth infection.

Experimental subcutaneous infection of mice with *N. brasiliensis* stage 3 larvae induces a typical type-2 response that involves a dramatic remodelling of epithelial cell populations, with goblet cell hyperplasia visible as soon as 5 days post-infection [3,4]. *N. brasiliensis* L3 larvae first migrate from their injection site to the lungs, where they moult to the L4 stage and are coughed up before being swallowed to reach the intestines (day 2 post infection) where they mature and lay eggs (starting 5 days post-infection). The parasite induces a rapid and robust type 2 response, resulting in worm expulsion by 6-8 days post infection.

While the doublecortin-like kinase 1 (Dclk1)-expressing tuft cell lineage represents only 0.4% of intestinal epithelial cells in naïve mice, with a relatively even distribution from the duodenum to the colon [5], we found that *N. brasiliensis* infection resulted in a 8,5 fold expansion in tuft cells (Fig. 1a, 1b). Tuft cell expansion was first detected by 5 days postinfection in intestinal crypts where proliferative epithelial progenitor cells reside, and then populated the villi by 7 days post infection (Fig. 1c, Extended data Fig. 1a). The kinetics of tuft cell expansion was equivalent to that of goblet cells (Fig. 1d, Extended data Fig. 1b).

Neo-differentiated tuft cells were indistinguishable from tuft cells present in naïve mice, as evaluated by expression of established tuft cell markers, including Dclk1, Sry-related transcription factor 9 (Sox9), phospholipase C gamma 2 (Plcγ2) (Extended data Fig. 1c) [6–8]. All tuft cells, characterised by Dclk1 and Growth factor independent 1b (Gfi1b) [8] expression also co-expressed the Pou domain, class 2, transcription factor 3 (Pou2f3) (Fig. 2a). In addition, rare (<3%, n=400 cells counted) $Pou2f3^{+}$;$Dclk1^{low}$ or even $Pou2f3^{+}$;$Dclk1^{-}$ cells were found at the base of crypts and likely represent early differentiating tuft cells, since villus $Pou2f3^{+}$ cells always co-express Gfi1b and Dclk1. Following infection, the percentage of proliferating tuft cells in crypts increased from 13±5,6% to 24±14,9% (p=0,035), indicating that cell proliferation contributes to the amplification of the tuft lineage during type 2 responses (Extended data Fig. 1d, 1e). Examination of the location of tuft cells present in *N. brasiliensis*-infected mice revealed that some tuft cells differentiate within or just above the stem cell zone (Extended data Fig. 1d), suggesting that biased differentiation from the recently described $Lgr5^{+}$ slowly cycling early secretory progenitors [9] or from the $Dll1^{+}$ secretory progenitor [10] also contributes to tuft cell lineage amplification. This hypothesis is supported by our finding that the differentiation of enteroendocrine cells expressing the insulinoma-associated 1 (*Insm1*) marker [11], another secretory lineage of the intestinal epithelium, is significantly (p=0.003) reduced (Extended data Fig. 1f, 1g) concomitantly to tuft cell amplification. The reduced number of enteroendocrine cells in infected mice also indicates that the increase in tuft cells is not due to a non-specific amplification of all secretory cell lineages.

To determine whether the increase in the tuft cell population following infection with *N. brasiliensis* was specific to C57BL/6 mice, we infected BALB/c mice and also observed a significant increase (14 fold, p<0.0001) in tuft cell numbers (Extended data Fig 2a, 2b).

Moreover, this response appears to be a common adaptation to helminth infection in general, as infection of C57BL/6 and BALB/c mice strains with *Heligmosomoides polygyrus* {Reynolds, 2012 #1791} also resulted in a significant increase (6.09 fold; $p<0.0001$ and 8.25 fold; $p<0.0001$, respectively) in tuft cell numbers (Extended data Fig. 2c, 2d). Tuft cell hyperplasia following *N. brasiliensis* infection occurred in *Rag*$^{-/-}$ mice (9.95 fold; $p<0.0001$) and therefore does not require functional T or B lymphocytes (Extended Data Fig. 2e, 2f).

Epithelial remodelling following helminth infection includes goblet cell hyperplasia and changes in mucus composition, and is associated with protective type 2 immunity [13]. Notably, goblet cell hyperplasia plays a more prominent role in immunity to *N. brasiliensis* infection than mast cells and IgE [14]. To investigate the role of tuft cells in this process, we identified and characterised a tuft cell-deficient mouse line. Mice deficient for the Pou2f3 transcription factor lack all Pou2f3-expressing taste receptor cells including sweet, umami and bitter taste cells [15], as well as Trpm5-expressing chemosensory cells in the nasal cavity [16] and olfactory epithelium [17]. The expression of Pou2f3 in tuft cells prompted us to analyse *Pou2f3*-deficient mice for this cell lineage. This revealed a unique phenotype in the intestinal epithelium, with a complete absence of tuft cells as assessed by the absence of Pou2f3, Dclk1, and Sox9 expression (Fig. 2b). The stem cell compartment, proliferation zone, and differentiation of enterocytes, goblet, enteroendocrine and Paneth cells were not affected (Fig. 2c and extended data Fig. 3). Furthermore, the distribution of immune cells in lymph nodes, mesenteric lymph nodes, spleen and *lamina propria* of *Pou2f3*$^{+/+}$ and *Pou2f3*$^{-/-}$ mice was equivalent (Extended data Figure 4) and lymphocytes were capable of responding to immune stimulation (Extended data Figure 5). Therefore, the absence of Pou2f3 does not affect global immunity or intestinal epithelium formation. Rather, Pou2f3 represents the first identified transcription factor that is specifically required to specify the presence of the tuft cell lineage in the intestinal epithelium, analogously to Sox9 for Paneth [18] and Ngn3 for enteroendocrine [19] cell lineages. Thus, *Pou2f3*$^{-/-}$ mice represent a powerful model to study the function of tuft cells.

Pou2f3$^{+/+}$ and *Pou2f3*$^{-/-}$ mice were infected with *N. brasiliensis* by subcutaneous injection of L3 larvae and the outcome of infection was assessed at several time points. Nine days after infection, few worms were found in *Pou2f3*$^{+/+}$ mice, indicating a nearly complete parasite expulsion (Fig. 3a). In sharp contrast, numerous worms were found in *Pou2f3*$^{-/-}$ mice (Fig. 3a), not only in the most proximal part of the small intestine, their normal site of attachment [20], but also in more distal locations. Importantly, more distally localised worms appeared healthy, and were mobile when transferred to culture medium. Together, these data strongly suggest that a compromised type-2 response is responsible for the prolonged worm survival in *Pou2f3*$^{-/-}$ tuft cell-deficient mice, and allows the worm infection to spread to more distal regions of the small intestine. This was confirmed by the analysis of mice 13 days after infection, where adult worms were almost absent (a single worm detected in a single mouse) in the intestinal mucosa of *Pou2f3*$^{+/+}$ mice (Fig. 3a), whereas numerous living adult worms were still found in the small intestine of *Pou2f3-deficient* mice (Fig. 3a).

To understand the mechanisms underlying the delayed worm expulsion in *Pou2f3*-deficient mice, we analysed the type-2 response-dependent remodelling of the intestinal epithelium 7

days after infection, a time point at which adult worms were detected in all infected animals. As predicted, tuft cells were completely absent in *Pou2f3*$^{-/-}$ mice (Fig. 3b). In *Pou2f3*$^{+/+}$ mice, the intestinal epithelium displayed extensive and generalised goblet cell hyperplasia, with large mucus vacuoles, and tuft cell hyperplasia (Fig. 3b). In contrast, *Pou2f3*$^{-/-}$ mice were devoid of overt goblet cell hyperplasia, with focal and moderate hyperplasia limited to the most proximal small intestine, and still exhibiting lower goblet cell numbers than WT mice (Fig. 3b, Extended Data Fig. 6a, Supplementary information 1 and 2). Therefore *Pou2f3*$^{-/-}$ tuft cell-deficient mice have a delayed type 2 response, with deficient mucosal goblet cell hyperplasia and delayed control of *N. brasiliensis* infection.

The goblet cell-produced Resistimlike beta (Retnlβ) molecule, strongly induced by type 2 cytokines, has direct anti-helminth activity that facilitates expulsion, especially for humen-dwelling helminths such as *N. brasiliensis* [3,21]. To investigate the molecular mechanism involved in the differential expulsion in *Pou2f3*$^{+/+}$ and *Pou2f3*$^{-/-}$ animals, we compared expression of Retnlβ in WT and *Pou2f3*$^{-/-}$ mice 7 days after *N. brasiliensis* infection, when worm expulsion starts in WT mice. Retnlβ was strongly expressed in hyperplastic goblet cells in *Pou2f3*$^{+/+}$ mice, but was only weakly expressed in *Pou2f3*$^{-/-}$ tuft cell-deficient mice (Fig. 3b, 3c, Extended Data Fig. 6a). Moreover, while IL4 levels were equivalent in mucosal tissue of *N. brasiliensis*-infected *Pou2f3*$^{+/+}$ and *Pou2f3*$^{-/-}$ mice, IL13 levels were markedly decreased in the latter (Fig. 3c). As both IL4 and IL13 type 2 cytokines are known to regulate Retnlβ expression [3], and IL4 is dispensable during type 2 responses to *N. brasiliensis* [22], our data strongly suggest that defective IL13 production is responsible for the decreased Retnlβ expression in *N. brasiliensis*-infected *Pou2f3*$^{-/-}$ mice. Thus, we identify a defective IL13/Retnlβ axis in tuft cell-deficient mice with impaired worm expulsion.

Based on these results, we next studied the link between tuft cells and type-2-mediated mucosal adaptation following *N. brasiliensis* infection. The goblet cell hyperplasia occurring upon helminth infection is intrinsically connected to type 2 immune responses because they both rely on IL4Rα signalling [3,23]. In accordance, deletion of the *Il4ra* gene either globally [24] or in non-haematopoietic cells alone [23] abrogates *N. brasiliensis*-expulsion. Importantly, the *N. brasiliensis*-induced tuft cell hyperplasia occurring in WT mice 7 days post infection was absent in *Il4ra1*$^{-/-}$ mice (Fig. 3d, Extended Data Fig. 6b). These data demonstrate the critical role of IL4Rα signalling in the expansion of the tuft cell population following helminth infection.

We then examined whether IL4Rα signalling is sufficient to trigger tuft cell lineage hyperplasia even in the absence of helminth infection. IL4Rα can be activated by IL4 as well as IL13, through type I (IL4Rα/γ) and type II (IL4Rα/IL13Rα1) receptors, respectively. We therefore injected naive C57BL/6 mice with rIL4/rIL13 for 5 days and assessed the histology of the intestinal epithelium. rIL4/rIL13 injection induced goblet cell hyperplasia together with a significant tuft cell expansion (Extended data Figure 6c). Importantly, treatment of *Pou2f3*$^{-/-}$ mice with rIL4/rIL13 also resulted in goblet cell hyperplasia, as well as Paneth cell hyperplasia, indicating a function of tuft cells upstream of IL4/IL13 Extended Data Fig. 6d). Moreover, ectopic IL4/IL13 induced Retnlβ expression in goblet cells, independently of the *Pou2f3* genotype. Retnlβ expression was found predominantly in crypts and was therefore delayed compared to the onset of goblet

cell hyperplasia (Extended data Figure 6c), and quantitatively lower than in an infectious context (Fig. 3b). Thus, our data show that IL4Rα signalling is sufficient to induce an expansion of the tuft cell lineage. Furthermore, ectopic stimulation of this signalling cascade obviates the need for tuft cells in the epithelial cell remodelling of the intestine, including induction of Retnlβ expression by hyperplastic goblet cells.

To determine whether the IL4/IL13-induced goblet cell hyperplasia was epithelial cell-autonomous, we used an *ex vivo* organoid culture system [25] that allows physiological responses of an isolated intestinal epithelium to be analysed in the absence of stromal cues. As expected, organoid cultures from *Pou2f3*$^{-/-}$ intestinal epithelia demonstrated an absence of tuft cells (Extended data Figure 7a). Moreover, in WT organoids, the tuft cell population increased as early as 48 hours following addition of ectopic IL4/IL13 (Extended Data Fig. 7b). Treatment with rIL4 alone or rIL13 alone yielded identical results to the rIL4/rIL13 mixture (Extended data Fig. 7c). Treatment of *Pou2f3*$^{-/-}$ organoids with rIL4/rIL13 also triggered goblet cell hyperplasia equivalent to that detected in *Pou2f3*$^{+/+}$ organoids, as indicated by Retnlβ expression (Extended data Figure 7d), revealing the critical role of type 2 cytokine signalling downstream of the tuft cell lineage. Furthermore, these data demonstrate that the intestinal epithelial response to IL4/IL13 is epithelium-autonomous and does not require additional stromal signals. Together, our data identify a novel function of tuft cells in initiating the mucosal type 2 responses with a positive feedback loop through IL13-producing immune cells that, in turn, amplifies the tuft cell lineage.

Finally, we investigated the physiological function of the observed tuft cell hyperplasia. This is fully established 7 days pos-infection, coincident with the start of worm expulsion. IL25 is an alarmin molecule produced by intestinal epithelial cells, capable of initiating type 2 responses by stimulating ILC2 cells to produce IL4 and IL13 [26,27]. However, the IL25-expressing epithelial cell type has not been identified. We thus analysed *IL25* mRNA expression in *Pou2f3*$^{+/+}$ and *Pou2f3*$^{-/-}$ mice infected with *N. brasiliensis*. Nine days after infection, *IL25* expression was higher in the intestinal mucosa of *Pou2f3*$^{+/+}$ mice than in that of *Pou2f3*$^{-/-}$ mice, where tuft cells are absent (Fig. 4a). This prompted us to analyse the role of tuft cells in IL25 expression. Tuft cell-restricted IL25 expression was observed in naïve mice (Fig. 4b, Extended Data Fig. 8b) and validated with detection of *IL25* mRNA expression in a FACS-enriched tuft cell fraction, but not in the rest of the intestinal epithelium (Fig. 4c, Extended Data Figure 8a). During infection with *N. brasiliensis*, IL25 expression remained restricted to tuft cells (Fig. 4b). Concomitant with tuft cell hyperplasia, epithelial IL25 expression peaks 9 days after infection with *N. brasiliensis*, at the time of worm expulsion, for which it is required [28]. Finally, treatment of *N. brasiliensis*-infected *Pou2f3*$^{-/-}$ mice with rIL25 almost completely rescued the absence of tuft cells and consequent delay in worm expulsion (Fig 4d). IL25 thus provides a mechanistic link between tuft cells, promotion of type 2 responses and worm expulsion, and their defects in tuft cell-deficient mice.

Taken together, our data reveal a critical function of tuft cells in initiating mucosal type 2 responses following infection with helminths through IL25 secretion. In the absence of tuft cells, IL25 and IL13 expression remain low, and type 2 mucosal responses and worm expulsion are delayed. This demonstrates that tuft cells initially function upstream of IL4/

IL13, but these cytokines in turn drive tuft cell hyperplasia, thus amplifying the response in a feed-forward loop to orchestrate rapid and effective anti-helminth immunity (Fig. 4e).

Methods

Animal strains

The *Pou2f3*-deficient mice (*Pou2f3tm1Abek*) have been previously described [15]. *Il4ra*-deficient mice [29] were kindly provided by Manfred Kopf (Basel Institute for Immunology, Switzerland). C57BL/6 and BALB/c mice were obtained from Charles River Laboratories. All the mice were maintained in an SPF animal facility and were naïve prior to the experiments. All animal experiments were approved by the Institutional Animal Care and Use Committee of Monell Chemical Senses Center or by the French Agriculture and Forestry Ministry. Unless specified, all mice were on a C57BL/6 genetic background. Mice were analysed at 10 weeks of age, regardless of the sex, with no randomization. For comparisons of KO and WT mice, littermates were analysed. At least 3 mice per condition were analysed in all experiments.

Immunophenotyping and flow cytometry analyses

Cells, isolated from peripheral lymph nodes, mesenteric lymph nodes, spleen and lamina propria were stained with Sytox blue or Live/dead fixable viability dye (Life technologies and eBioscience respectively) together with the appropriate conjugated αCD3, αCD45.2, αCD62L, αCD4, αCD8, αCD44, αTCRγδ, αCD19, αNK1.1, αGrl, αCD11b, αCD11c, and αFoxp3 (eBioscience or Becton Dickinson, San Diego, CA).

IL6, IL12, TNFβ, IL-10, MCP-1 and IFNγ production was assessed in the culture supernatant of LPS/IL4-activated splenocytes using a Cytometric Bead Array (CBA) Kit (BD Biosciences). To assess intracellular cytokine production, freshly isolated and anti-CD3/CD28 stimulated LN cells were activated with PMA (Sigma-Aldrich; 100 ng/ml)/ Ionomycin (Sigma-Aldrich; 1 μg/ml) in the presence of brefeldin A (Sigma-Aldrich; 10ug/ml) for 4h at 37°C, fixed, permeabilized and then stained with specific antibodies against IL2 and IFNγ.

Foxp3 staining was performed following fixation/permeabilization (eBioscience). Stained cells were assessed by flow cytometry (LSR Fortessa, Becton Dickinson, San Jose, CA) and data were analyzed by FACSDiva (v.8.0, BD Biosciences) and FCAP Array Software (CBA analysis).

Ex vivo stimulations

LN cell activation was performed using plate-bound anti-CD3 (clone 2C11; 1 μg/ml) and anti-CD28 (clone PV-1 1 μg/ml) mAbs in RPMI 1640 media (Life Technologies) supplemented with 10% FCS, 2mM glutamine and 1% Penicillin/streptomycin. Exogenous IL2 (100 U/ml) was added every other day starting at day 2 post-activation. Cell proliferation was monitored by labelling with CFSE (Life Technologies; 2.5 μM) for 3 min at RT. Splenocytes were activated with LPS (20 μg/ml) and IL-4 (25 ng/ml). Supernatants were collected 40 hours following activation.

Europe PMC Funders Author Manuscripts

Immunoglobulin detection

IgG detection in supernatants of LPS/IL4-stimulated splenocytes was assayed by ELISA. Microtiter plates (Maxisorb, Nunc) were saturated O/N at 4 °C with 100 µl of anti-IgG2a, anti-IgG2b, anti-IgA antibodies or anti-IgG (Fab'2) resuspended in PBS (5µg/ml). Plates were washed 3 times with 0.1% Tweemcontaining PBS (PBST). Samples (1/2 dilution) were diluted in a final volume of 100 µl/well of PBST-1%BSA and incubated for 2h at RT. Following washes, peroxidase-∞njugated anti-mouse anti-IgG2a, anti-IgG2b, anti-IgA (Serotech) or anti-IgG gamma-chain (SIGMA) antibodies were added in PBST-1%BSA (1:1000 dilution; 100 ul/well) and incubated for a 1 hour at 37°C. Immunoglobulin levels were then revealed with *o*-phenylenediamine (Sigma; 4 µg/ml) in 0.1 M Na citrate and 003% hydrogen peroxide. Absorbance was measured at 450 nm using an automated plate reader (InfiniteM200Pro, TECAN) after 5 min at room temperature.

Tuft cells sorting

Freshly isolated small intestines of BC57BL/6 mice were flushed with PBS and incised along their length. The tissue was then incubated in 30mM EDTA (Sigma) in HBSS pH 7.4 (Life Technologies) on ice, and transferred in DMEM (Life Technologies) supplemented with 10% FBS (Sigma). Vigorous shaking yielded epithelial fraction that was then incubated with 100ul of Dispase (BD Biosciences) in 10 ml of HBSS, supplemented with 100ul of DNAse I at 2000 Kunitz (Sigma). Single cell preparation obtained by filtration on a 30 uM mesh was incubated with a Phycoerythrin Rat anti-mouse Siglec-F antibody for 30 minutes at 4°C (BD pharmigen 552126), washed with HBSS and resuspended in appropriate volume of HBSS pH 7.4 supplemented with 5% FBS before staining with 7-AminoActinomycin D (Life Technologies) to exclude dead cells. Siglec-F^+ live cells were sorted using a FACSAria (Becton Dickinson).

Parasite infections

Pou2f3$^{+/+}$, *Pou2f3*$^{-/-}$, *Il4ra*$^{+/+}$ and *Il4ra*$^{-/-}$, C57BL/6 and BALB/c WT mice were used for N. brasiliensis infection experiments. Mice were infected with 250 L3 infective *N. brasiliensis* larvae by sub-cutaneous injection [20] or with 200 L3 *H. polygyrus* L3 larvae by gavage. Infection parameters were monitored by enumeration of live adult worms in the small intestinal tissue by two different investigators blinded to the study groups.

Reagents

Recombinant murine IL4 (214-14), recombinant murine IL13 (210-13) were purchased from PeproTech, and recombinant murine IL25 (1399) was from R&D Systems. For animal treatment, mice were I.P. injected daily with a mixture of both interleukins or with rIL25 (40µg/kg of body weight). For rescue experiments in *Pou2f3*$^{-/-}$ mice, rIL25 was injected from day 3 post-infection.

Organoid culture

Organoid culture were performed as previously described [25] using intestinal crypts from *Pou2f3*$^{+/+}$, *Pou2f3*$^{-/-}$ or C57BL/6 WT mice. Organoid lines were passaged up to 10 times before experiments to ensure pure epithelial cultures. When indicated, cultures were

stimulated with recombinant murine IL-4 (400ng/ml), recombinant murine IL-13 (400ng/ml) or an equimolar mixture of the two cytokines. For histological studies, organoids were washed twice in cold PBS to dissolve the matrigel, fixed overnight in neutral-buffered formalin at 4°C and included in Histogel (Thermo Scientific) before paraffin embedding (n=3 experiments from independent mice).

RNA extraction and PCR

Total RNA from intestinal organoids or snap frozen intestinal tissues was isolated using TRIzol (Invitrogen) followed by precipitation with isopropanol. Further RNA purification was carried out on RNeasy columns (Qiagen, 74104) and DNase treatment. Reverse transcription was performed with 500ng-2μg of purified RNA using Transcriptor First Strand cDNA synthesis KIT (Roche) according to the manufacturer's instructions. For qRT-PCR experiments, gene expression was quantified on the LightCycler 480 using LightCycler 480 SYBR Green I Master (Roche). The results from three independent organoid cultures were normalized to the expression level of *Gapdh* and *Hprt* and relative expression was obtained using the ΔΔCt method. Primer sets for each gene are listed in Extended data table 1. PCR analyses were performed on an Eppendorf Mastercycler, using the primer sets listed in the Extended data information 1 table.

In situ hybridisation

Single colorimetric and double fluorescent *in situ* hybridisation analyses were carried out as described previously [30]. Briefly, digoxigenin- and fluorescein-labeled antisense RNAs were synthesized and used as probes after fragmentation to about 150 bases under alkaline conditions. Small intestines were dissected from mice shortly after euthanasia and embedded in frozen O.C.T. compound (Sakura Finetech). Fresh-frozen sections were prepared using a cryostat (CM1900, Leica Microsystems), fixed with 4% paraformadehyde, hybridized with probe(s), and then washed under stringent conditions. Hybridized probes were immunohistochemically detected using alkaline phosphatase-conjugated anti-digoxigenin antibody (Roche Diagnostics) and biotin–conjugated anti-fluorescein antibody (Vector Laboratories). Signals were developed using 4-nitro blue tetrazolium chloride/5-bromo-4-chloro-3-indolyl-phosphate as chromogenic substrates for single colorimetric analyses or the Tyramid Signal Amplification method and HNPP Fluorescent Detection Set (Roche Diagnostics) for double-fluorescent analyses. Stained and fluorescent images were obtained on a Nikon eclipse 80i microscope (Nikon Instruments Inc.) equipped with a DXM1200C digital camera (Nikon) and a Leica SP2 confocal scanning microscope (Leica), respectively. RNA probes generated were as follows: nucleotides 72–2363 of Pou2f3 (accession no. NM_011139), nucleotides 1–2228 of Slc15a1 (accession no. BC116248), nucleotides 1–3255 of Muc2 (accession no. BC034197), nucleotides 1–1102 of Gcg (accession no. BC012975), nucleotides 1–584 of Gip (accession no. BC104314), nucleotides 27–400 of Defcr6 (accession no. M33225), nucleotides 1–1628 of Olfm4 (accession no. BC141127), nucleotides 1–2750 of Dclk1 (accession no. BC050903), and nucleotides 1–2797 of Ptgs1 (accession no. BC005573).

Fluorescent and bright-field immunohistochemistry on paraffin-embedded tissue

Tissue dissection, fixation, and immunohistochemistry on thin sections of paraffin-embedded tissue were performed essentially as described previously [5]. Primary antibodies used in this study were as follows: anti-Sox9 (AB5535; Millipore), anti-Cox1 (sc-1754; Santa Cruz), anti-PCNA (sc-56; Santa Cruz), anti-Plcγ2 (sc-5283, Santa Cruz), anti-Gfi1b (Sc-8559; Santa Cruz), anti Pou2f3 (sc-330, Santa Cruz and HPA019652, Prestige Antibodies), anti-Dclk1 (ab31704; AbCam), anti-Ki67 (ab16667; AbCam), anti-Retnlb (ABIN465494, Antibodies online), anti-IL25 (mAb 1258; R&D Systems). Anti-Insm1 was a gift from Dr. Carmen Birchmeier (Max-Delbrück-Center for Molecular Medicine; Berlin; Germany). Slides were washed twice times with 0.1% PBS-Tween (Sigma-Aldrich) before incubation with fluorescent secondary antibodies conjugated with either Alexa 488, Cyanim3, or Cyanim5 (Jackson ImmunoResearch Laboratories, Inc.) and Hoechst at 2 μg/ml (Sigma-Aldrich) in PBS–Triton X-100 0.1% (Sigma-Aldrich). Stained slides were washed again in PBS before mounting with FluoroMount (Sigma-Aldrich). Methods used for bright-field immunohistochemistry were identical, except that Envision+ (Dako) was used as a secondary reagent. Signals were developed with DAB (Sigma-Aldrich) and a hematoxylin counterstain (DiaPath) was used. After dehydration, sections were mounted in Pertex (Histolab). Enterocytes-alkaline phosphatase activity was revealed with Fast-red substrate (Sigma-Aldrich). All stainings were repeated in at least 3 mice per group in 3 independent experiments and scored by three different investigators blinded to the study groups.

Microscopy and imaging

Fluorescent pictures were acquired at room temperature on an AxioImager Z1 microscope (Carl Zeiss, Inc.) equipped with a camera (AxioCam MRm; Carl Zeiss, Inc.), EC Plan Neofluar (5x, NA 0.16; 10x, NA 0.3; 20x, 0.5 NA; 100x, NA 1.3) and Plan Apochromat (40x, NA 0.95; 63x, NA 1.4) objectives, the Apotome Slider system equipped with an H1 transmission grid (Carl Zeiss, Inc.), and Axio-ision software (Carl Zeiss, Inc.).

Bright-field immunohistochemistry pictures were taken at room temperature on an Eclipse 80i microscope (Nikon) with Plan Fluor (10x, NA 0.3; 20x, NA 0.5; 40x, NA 0.75; and 60x, NA 0.5–1.25) lenses (Nikon) and a digital camera (Q-Imaging Retiga 2000R with a Q-Imaging RGB Slider). Pictures were captured with Q-Capture Pro software (Nikon). Post-treatment of pictures (level correction), annotations, and panel composition were performed using Photoshop software (Adobe).

Statistical analyses

Prism software was used for descriptive statistical analyses, including normal distribution, variance comparison, mean and standard deviation calculation. A two-sided Mann-Whitney test was used for quantifications of data presented in Fig. 1b, 2c, and Extended Data 1a, 1b, 1e, 1g, 2a, 2b, 2c, 4b, 4c, 4d, 5a, 5d, 5e. Individual data points are shown in Fig. 3a due to small sample size.

Extended Data

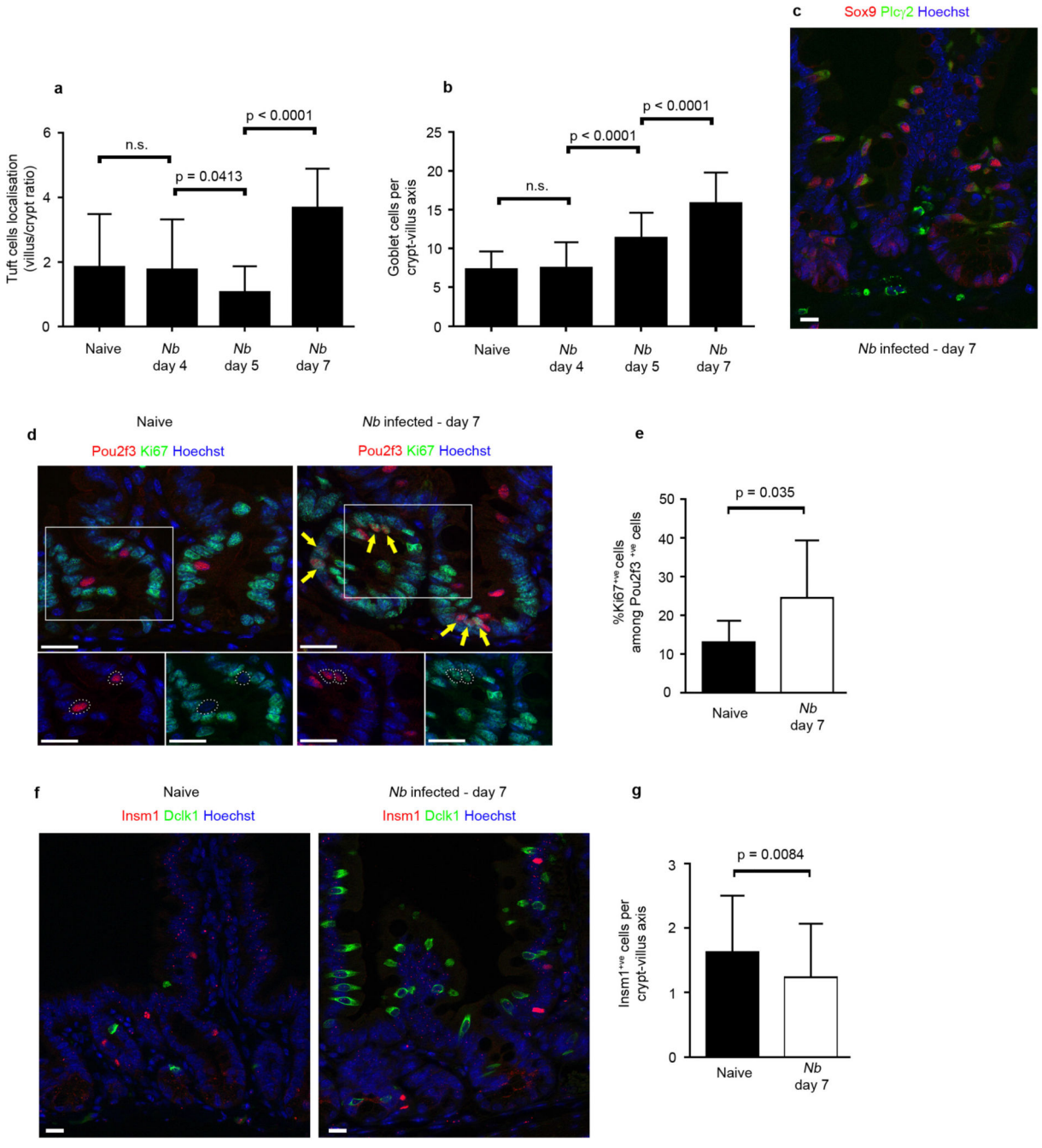

Extended Data Figure 1. Epithelial differentiation parameters during *Nb* infection.

a, Graph showing the distribution of Dclk1^{+} tuft cells in naive and infected mice 4, 5 and 7 days post infection. Cells were counted in the crypt and villus compartments of n = 50 crypt–villus units per mouse with 3 mice per condition. Means of villus/crypt ratio of tuft cell numbers are shown. **b**, Quantification of the goblet cell hyperplasia in naive and infected mice 4, 5 and 7 days post infection (n = 50 crypt–villus units per mouse; 3 mice

per condition). **c**, Neo-differentiating tuft cells following *Nb* infection are indistinguishable from the tuft cells found in naive mouse intestinal epithelium as shown with Sox9 and Plcγ2 stainings (n = 3 mice). **d**, Proliferation status of Pou2f3$^+$ tuft cells in naive and infected mice, shown with co-expression with the Ki67 proliferation marker. Arrows indicate Ki67$^+$ cells located at various positions along the crypt axis. **e**, Increased proliferation of Pou2f3$^+$ tuft cells during response to *Nb* infection (n = 3 naive and 3 infected mice). **f**, Dclk1$^+$ tuft cells and Insm1$^+$ enteroendocrine cells are distinct populations (n = 3 mice). **g**, Decrease of the Insm1$^+$ enteroendocrine cell population during type 2 responses to *Nb* infection, concomitant to the expansion of the tuft cell lineage 7 days post infection (n = 3 naive and 3 infected mice). All the histograms show means ± s.d. A two-tailed Student's t-test with Welch's correction was used, except for **g** where the 2 groups displayed comparable variances. All stainings were repeated 3 times.

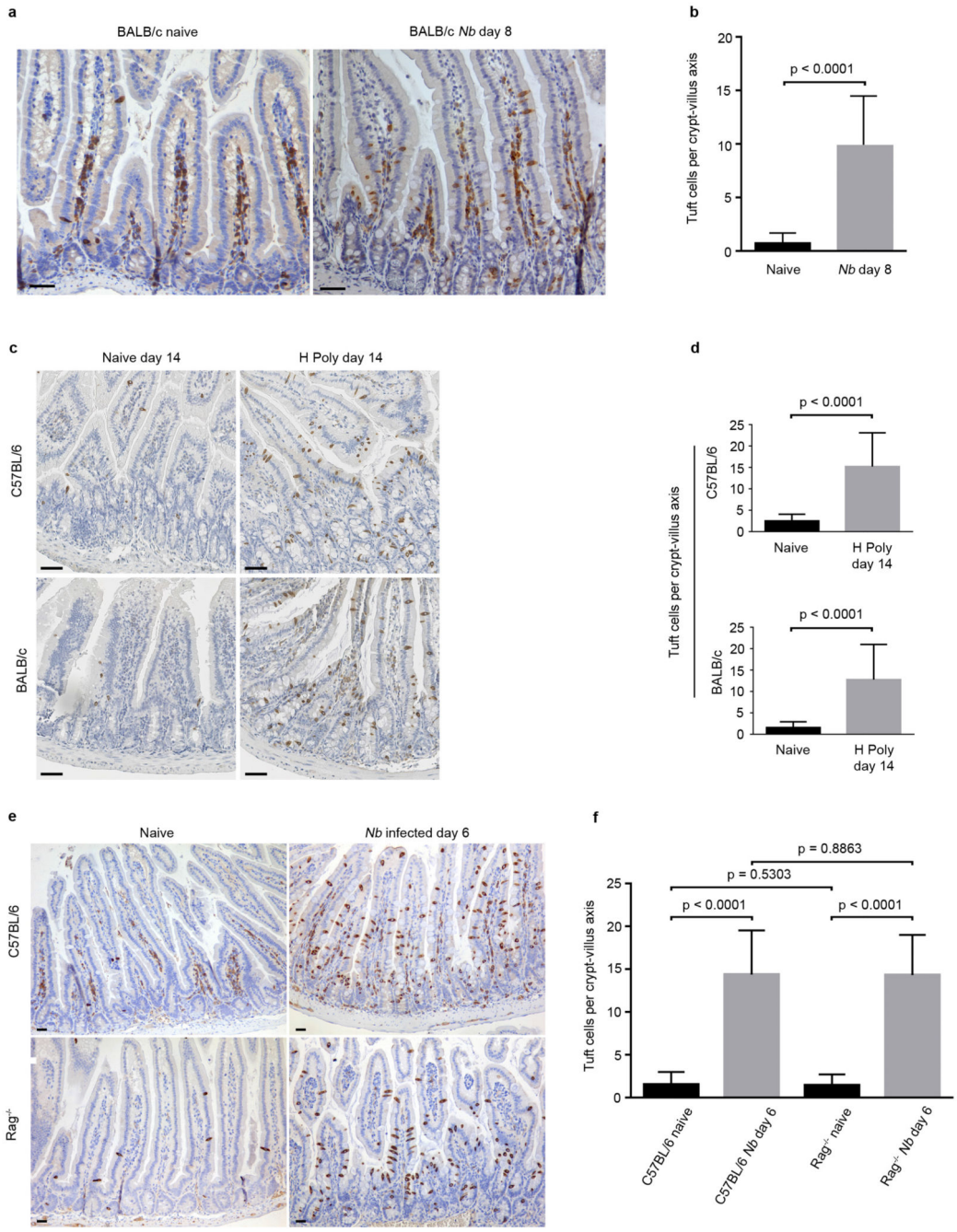

Extended Data Figure 2. Expansion of the tuft cell lineage is a common adaptation of the intestinal epithelium following infection with helminth parasites.

Tuft cell lineage expansion was assessed by Dclk1 immunohistochemistry in 2 different genetic backgrounds following infection with two different helminths, at the indicated time points. **a**, **b**, Naive and *Nb*-infected BALB/c mice. **c**, **d**, Naive and *H. polygyrus*-infected C57BL/6 and BALB/c mice. **e**, **f**, Naive and *Nb*-infected C57BL/6 and Rag$^{-/-}$ mice. **b**, **d**, **f**, n = 50 crypt–villus units per mouse; 3 mice per condition. Data are shown as means ± s.d.

Europe PMC Funders Author Manuscripts

and *P* values are indicated. A two-tailed Student's *t*-test with Welch's correction was used. Scale bars, 20 μm. All experiments displayed in this figure were repeated 3 times.

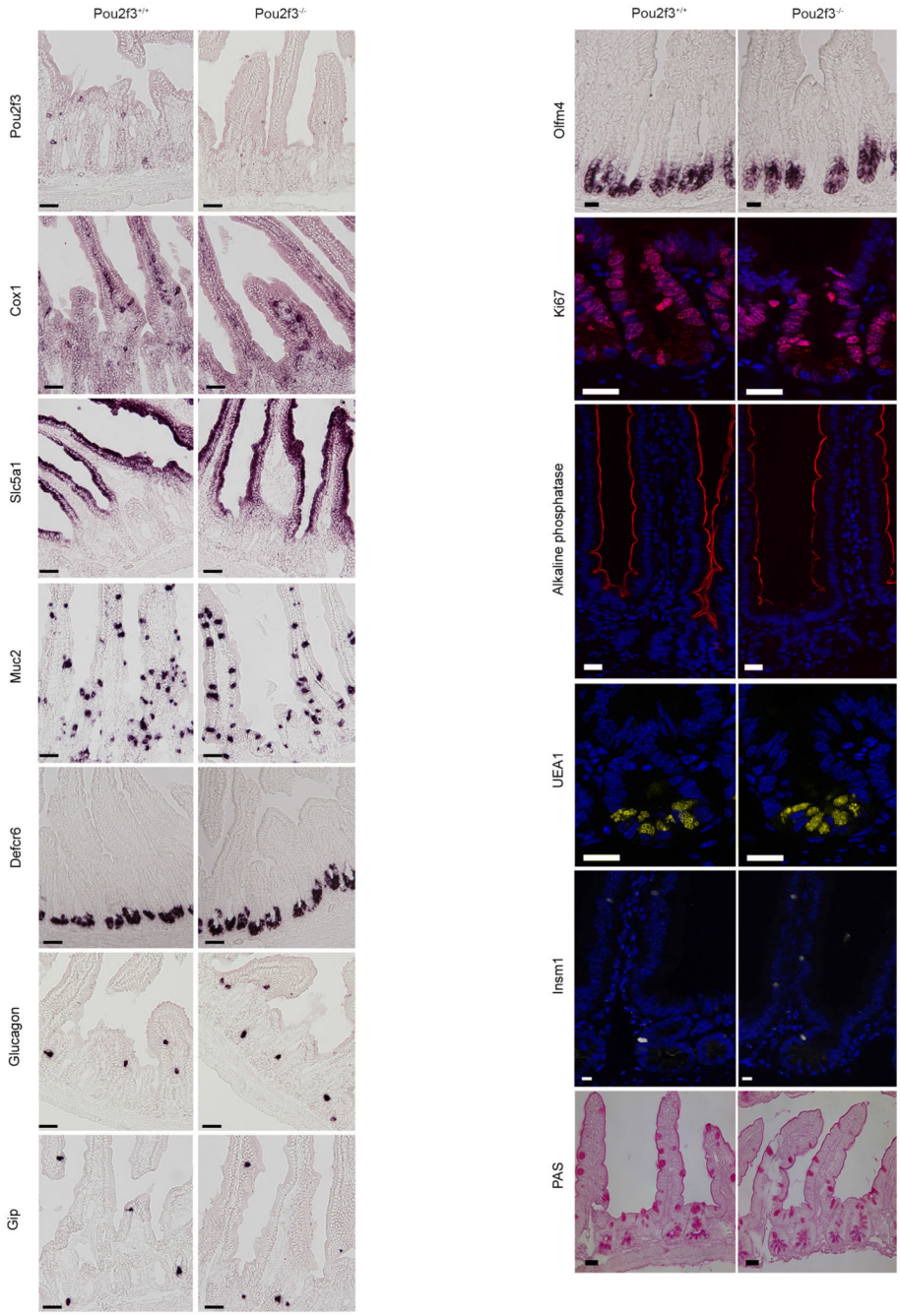

Extended Data Figure 3. *Pou2f3* deficiency results in the specific absence of tuft cells in the intestinal epithelium.

Characterization of the intestinal epithelium in *Pou2f3*-deficient mice as compared with wild-type littermate controls ($n = 3$ mice of each genotype). Left, *in situ* hybridization showing absence of tuft cells (*Pou2f3, Cox1*) in *Pou2f3*$^{-/-}$ mice, whereas enterocytes (*Slc5a1*), goblet cells (*Muc2*), Paneth cells (*Defcr6*) and enteroendocrine cells (glucagon,

Gip) are unaffected. Right, representative pictures of the *in situ* hybridization (*Olfm4*) and immunohistochemistry experiments underlying the quantitative analysis provided in Fig. 2c showing that the stem cells (Olfm4), proliferative compartment (Ki67), and differentiated cell types: enterocytes (alkaline phosphatase), Paneth (UEA1), enteroendocrine (Insm1) and goblet (PAS staining) cells populations are unaffected in the *Pou2f3*$^{-/-}$ mice. All panels show representative pictures of experiments replicated 3 times in 3 different mice. Scale bars, 20 μm.

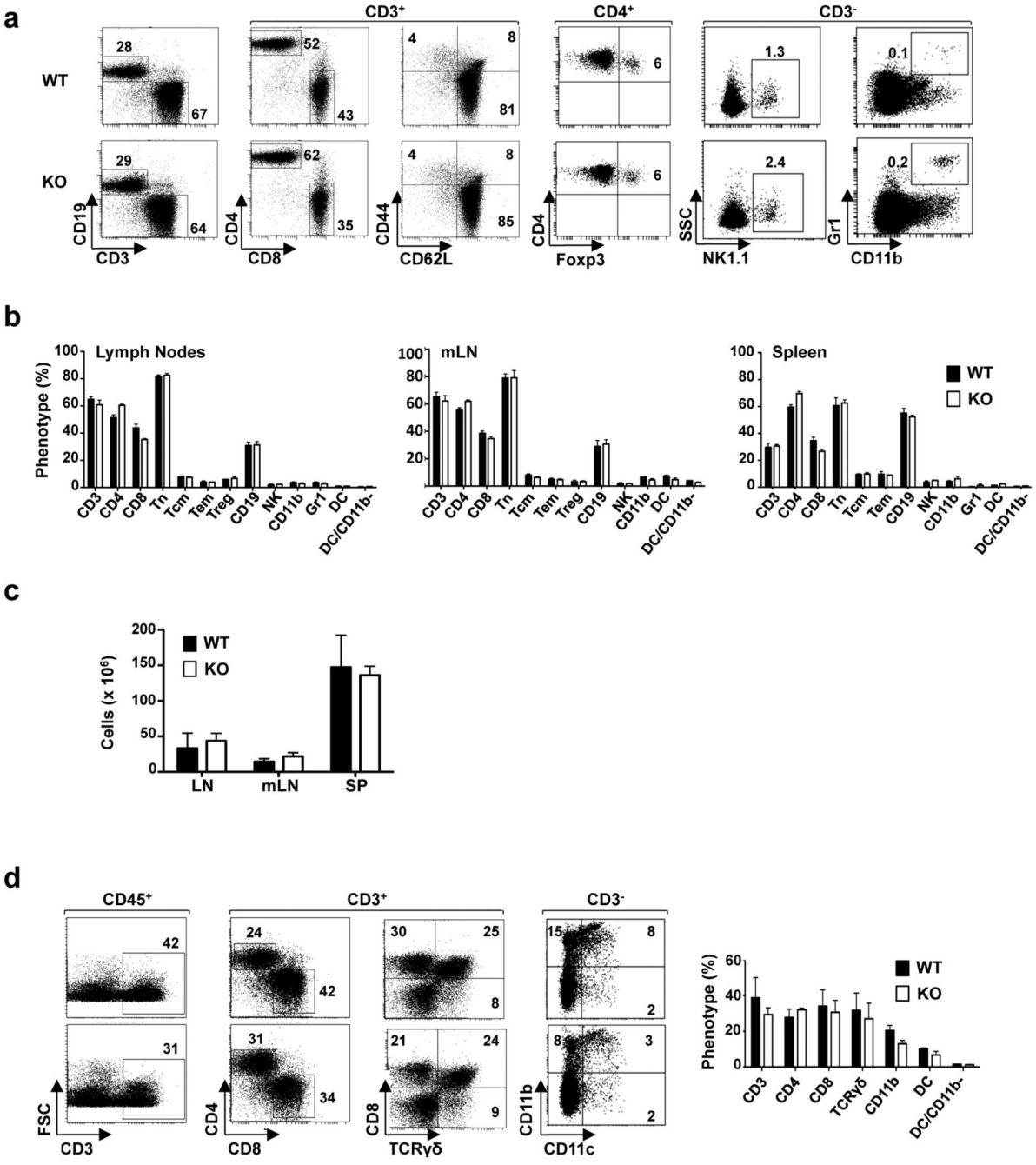

Europe PMC Funders Author Manuscripts

Extended Data Figure 4. Immune cell homeostasis is not altered in *Pou2f3*$^{-/-}$ tuft-cell-deficient mice.

a, The repartition of immune cells in wild-type and *Pou2f3*$^{-/-}$ mice was monitored by flow cytometry. The presence of T (CD3^{+}), B (CD19^{+}), CD4^{+}, CD8^{+}, naive (Tn; CD3^{+} CD62L^{+}CD44^{-}), central memory (Tcm; CD3^{+}CD62L^{+}CD44^{+}), effector memory (Tem; CD3^{+}CD62L^{-}CD44^{+}), regulatory (Treg; CD4^{+}Foxp3^{+}), natural killer (NK; CD3^{-}NK1.1^{+}) and myeloid (CD11b^{+}Gr1^{+}) cells was assessed by staining with fluorochrome-tagged antibodies and representative dot plots are shown. The percentages of positively-stained cells are indicated. **b**, Quantification of the different immune cells in lymph nodes (LN), mesenteric lymph nodes (mLN) and spleens (SP) of wild-type and *Pou2f3*$^{-/-}$ mice are presented. Data are means ± s.d. (n = 3 mice per genotype). **c**, Total cells in LN, mLN and SP of wild-type and *Pou2f3*$^{-/-}$ mice are presented as means ± s.d. (n = 3 mice per genotype). **d**, Immune lineage cells in the lamina propria of wild-type and *Pou2f3*$^{-/-}$ mice were monitored by flow cytometry after tissue dissociation. The percentage of T cells was assessed within the CD45^{+} haematopoietic gate, CD4, CD8 and gamma-delta T cells (CD8^{+}TCR-γδ^{+}) within the CD3^{+} gate and myeloid cells within the CD3^{-} gate, as indicated. Representative dot plots are presented (left). Quantification of immune cells within the lamina propria are shown as means ± s.d. (n = 3 mice per group). No significant differences were detected for all cell types between wild-type and *Pou2f3*$^{-/-}$ mice (P > 0.05). A two-tailed Student's t-test was used.

Europe PMC Funders Author Manuscripts

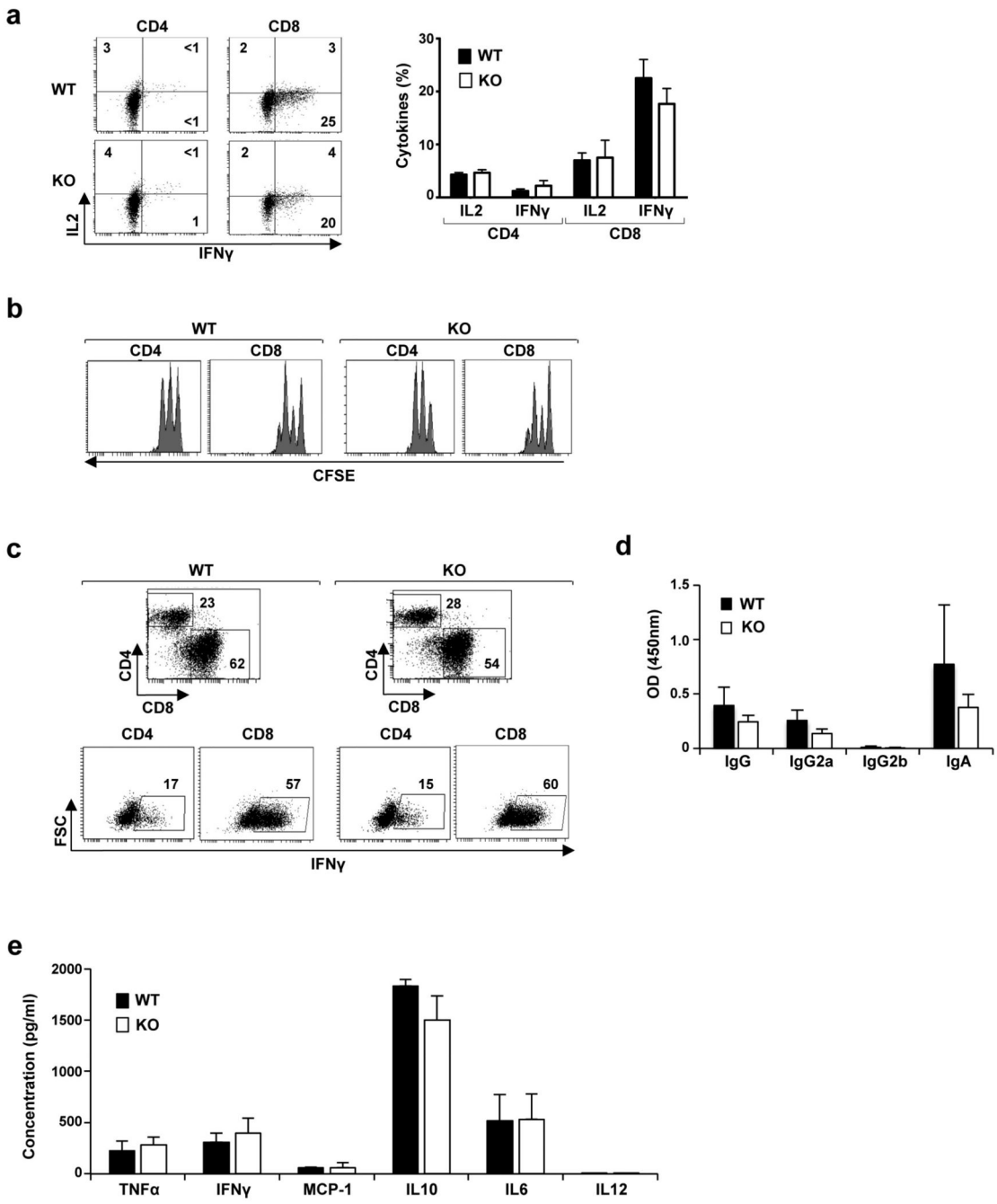

Extended Data Figure 5. Equivalent immune responsiveness of wild-type and *Pou2f3*$^{-/-}$ lymphocytes.

a, The level of IL-2 and interferon gamma (IFN-γ) production by *Pou2f3*$^{+/+}$ and *Pou2f3*$^{-/-}$ CD4 and CD8 lymph node T cells was monitored directly after *ex vivo* isolation and representative histograms are presented (left). Quantification of cytokine secreting CD4 and CD8 T cells are presented as means ± s.d. ($n = 3$ per group; $P > 0.05$). **b**, CFSE-loaded T cells were activated with immobilized anti-CD3/anti-CD28 antibodies for 2 days and proliferation was monitored as a function of fluorescence dilution. Representative

histograms for CD4 and CD8 T cells are shown. **c**, IFN-γ production in wild-type and *Pou2f3*$^{-/-}$ lymphocytes was assessed at day 6 post CD3/CD28 stimulation and representative plots for CD4 and CD8 T cells are presented. **d**, Splenocytes from wild-type and *Pou2f3*$^{-/-}$ mice were activated with LPS+IL-4 for 40 h and levels of secreted IgG, IgG2a, IgG2b and IgA were monitored by ELISA. Means ± s.d. are presented. **e**, Splenocytes were activated as above and levels of TNF-α, IFN-γ, MCP-1, IL-10, IL-6, and IL-12 were monitored by cytometric bead array. Means ± s.d. are presented. A two-tailed Student's *t*-test was used.

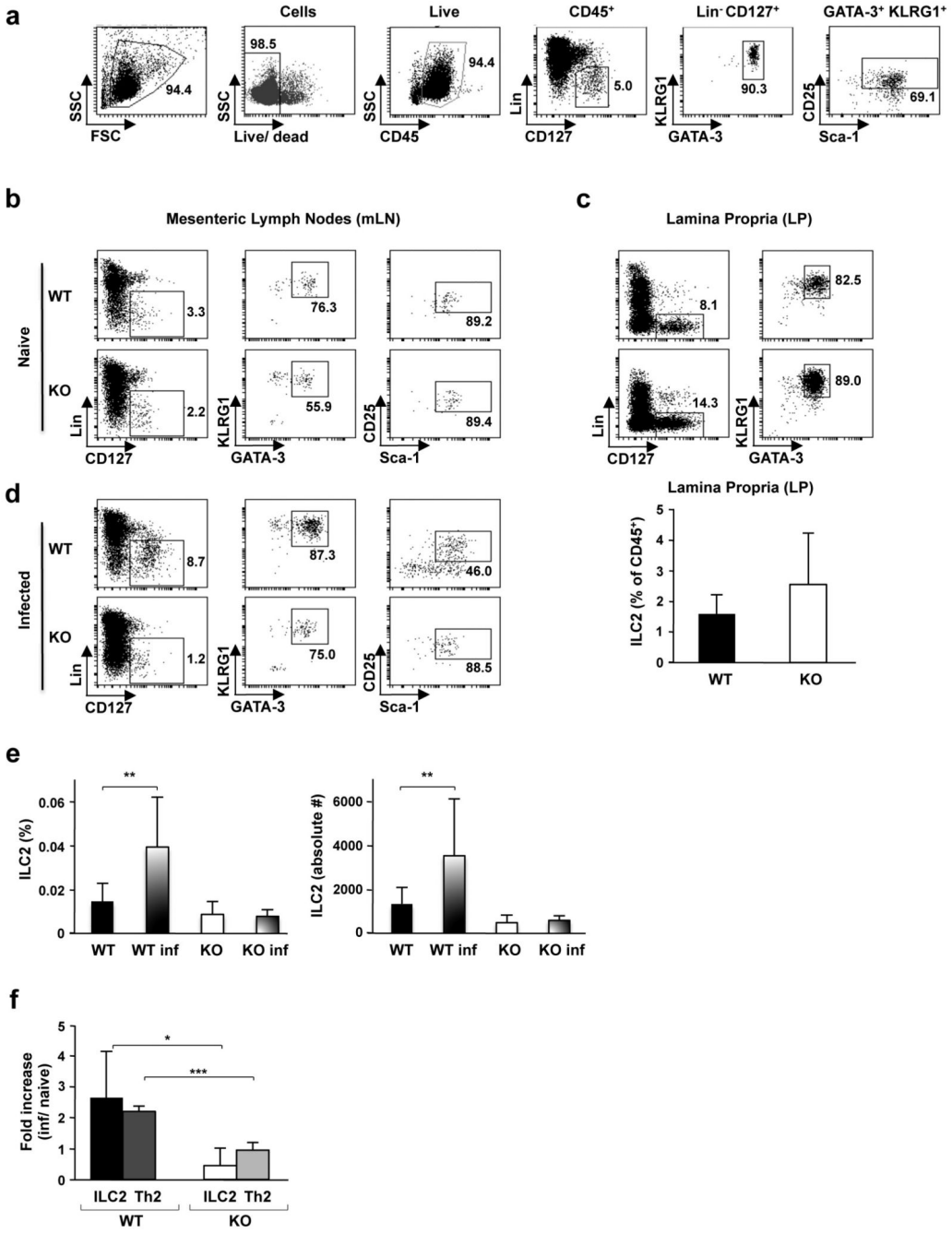

Europe PMC Funders Author Manuscripts

Europe PMC Funders Author Manuscripts

Extended Data Figure 6. Defective induction of type 2 immunity in *Pou2f3*$^{-/-}$ mice following helminth infection.

a, Flow cytometry gating strategy for analysis of the innate ILC2 subset is shown. ILC2s were assessed within the CD45^{+} haematopoietic subset as lineage-CD127^{+} cells expressing KLRG1, GATA-3, Sca-1 and CD25 cell surface markers. Numbers represent the percentages of boxed cells. The staining strategy was validated using mLN cells from ZAP-70$^{-/-}$ mice as this subset is present at relatively high levels in these immunodeficient mice. **b**, The presence of ILC2 cells in mLNs of naive *Pou2f3*$^{+/+}$ (WT) and *Pou2f3*$^{-/-}$ (KO) mice was assessed using the gating strategy shown above. Representative data from WT (n = 8) and KO (n = 5) mice are presented. **c**, Representative plots of ILC2 cells in lamina propria of naive WT (n = 7) and KO (n = 5) mice are shown (top). Quantifications of ILC2 are presented as means ± s.d. **d**, WT and KO mice were infected with *N. brasiliensis* and the presence of ILC2 in mLNs was assessed 5 days post infection. Representative plots are shown (n = 6 mice per group). **e**, Quantification of ILC2 cells in mLN of naive versus infected WT and KO mice. The percentage of ILC2s within the live gate (left) and the absolute numbers of ILC2s (right) are presented. Data are means ± s.d. (n = 5 for WT, n = 8 for KO, n = 6 for both groups of infected mice). $^{**}P$ = 0.01. **f**, The fold-increase in ILC2 (lineage^{-}CD127^{+}KLRG1^{+}GATA-3^{+}) and Th2 (CD3^{+}CD4^{+}Gata-3^{+}) cells in mLN was assessed as a function of infection (n = 6 per group). The mean fold-increase ± s.d. in WT and KO mice is presented. $^{*}P$ = 0.02, $^{***}P$ = 0.0005. A two-tailed Student's t-test was used.

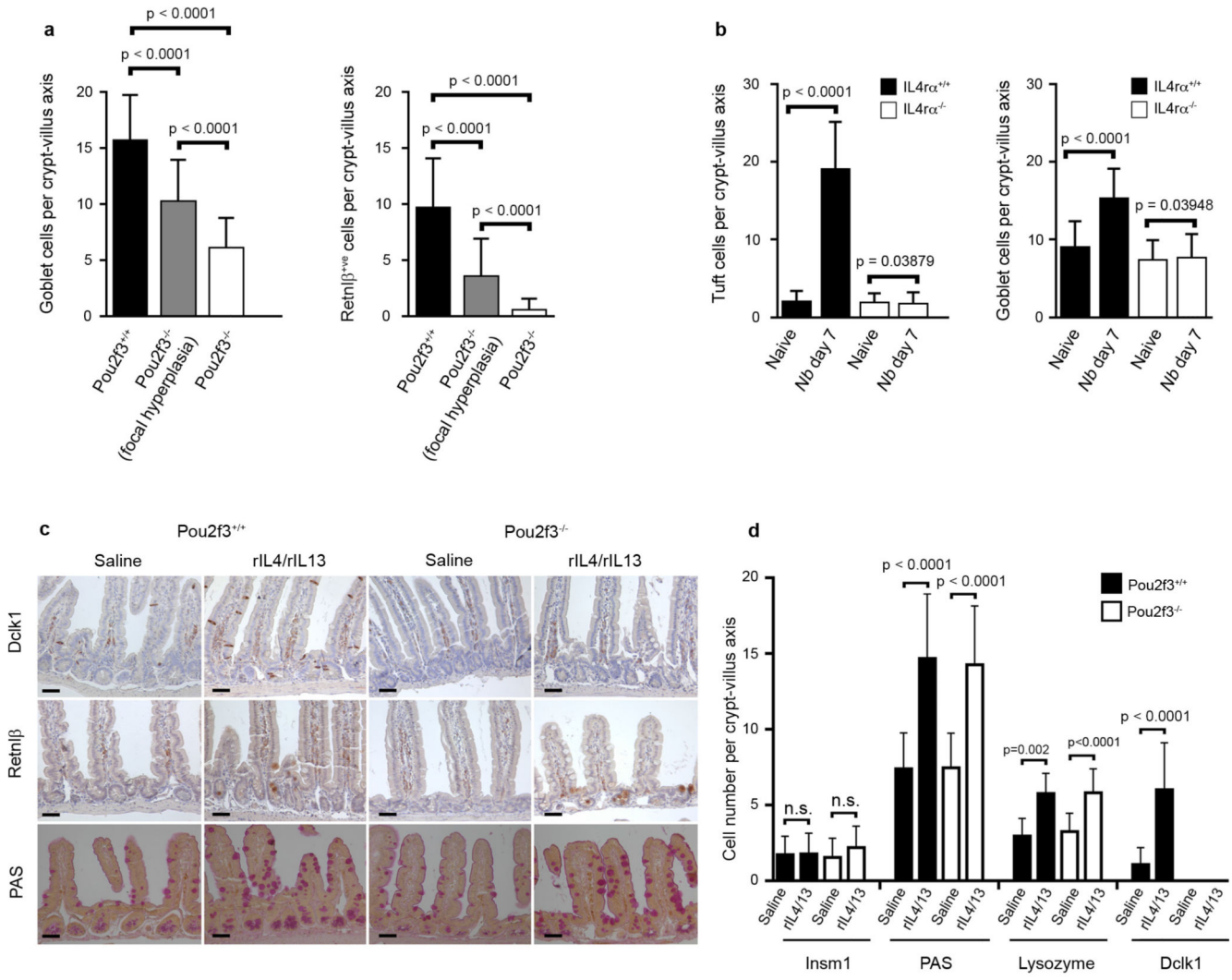

Extended Data Figure 7. Signalling via IL-4Rα is required and sufficient to induce goblet and tuft cell hyperplasia.

a, Quantification of goblet (PAS and Retnlβ staining) cells in *Pou2f3*$^{+/+}$ and *Pou2f3*$^{-/-}$ mice infected with *Nb* (day 7 post infection). In *Pou2f3*$^{-/-}$ mice, crypt–villus axes from both focally responding regions and the rest of the tissue were counted. **b**, Quantification of tuft cells (Dclk1 staining) and goblet cell hyperplasia (PAS) in *Il4ra*$^{+/+}$ and *Il4ra*$^{-/-}$ mice. **c**, Histological analysis showing tuft (Dclk1 staining) and goblet (PAS and Retnlβ staining) cells in *Pou2f3*$^{+/+}$ and *Pou2f3*$^{-/-}$ mice following treatment with a mixture of rIL-4 and rIL-13 for 5 days. $n = 3$ mice per condition. All panels show representative experiments replicated 3 times. Scale bars, 20 μm. **d**, Quantitative analysis of the changes in the different cell types of the intestinal epithelium of *Pou2f3*$^{+/+}$ and *Pou2f3*$^{-/-}$ mice following treatment with a mixture of rIL-4 and rIL-13 during 5 days. For **a**, **b**, **d**, $n = 50$ crypt–villus axes counted in 3 mice per genotype or condition. Data are shown as means ± s.d. and *P* values are indicated. A two-tailed Student's *t*-test with Welch's correction was used.

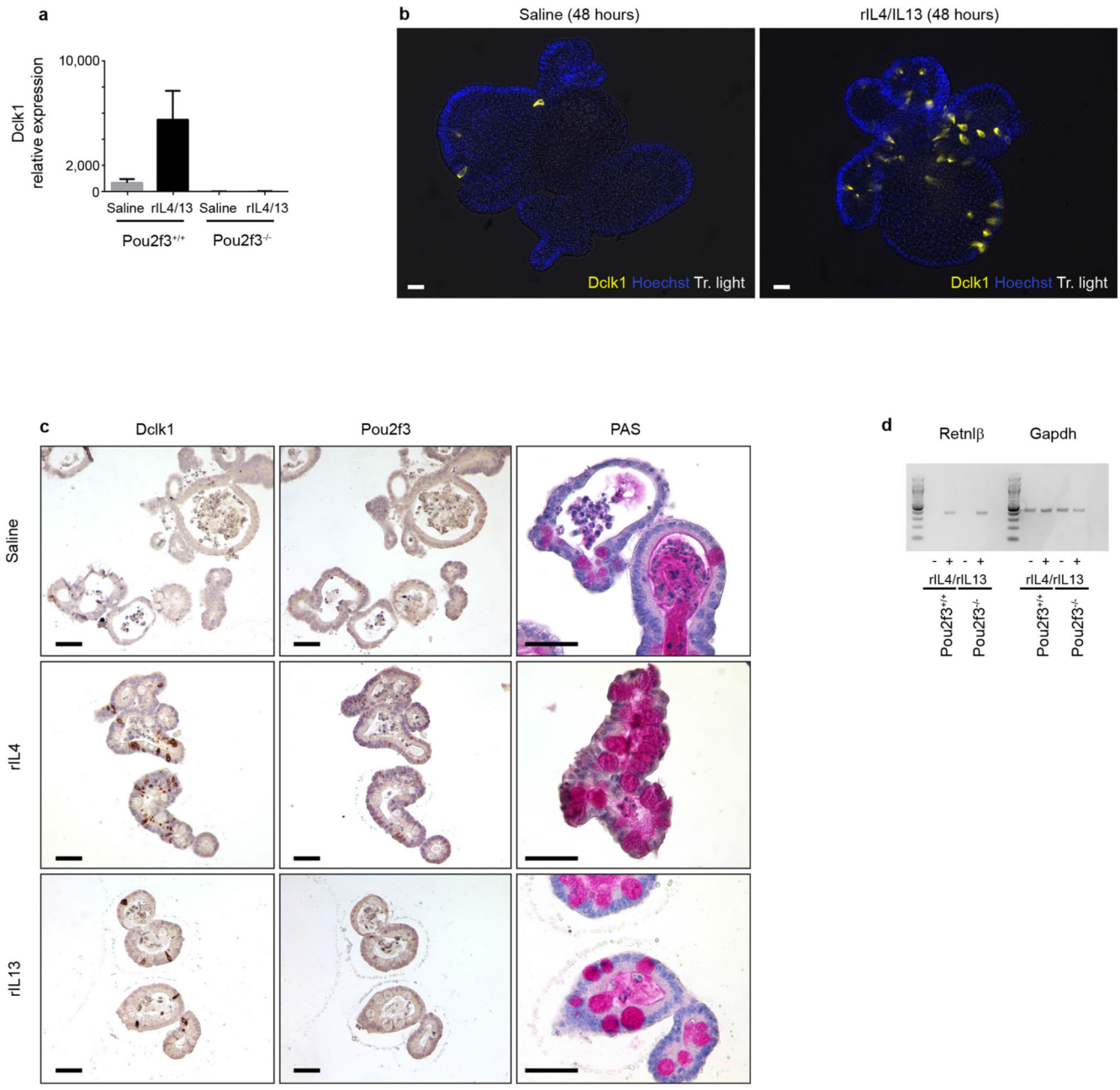

Extended Data Figure 8. Signalling via IL-4Rα is sufficient to induce goblet and tuft cell hyperplasia in mouse intestinal organoids.

a, Quantification of *Dclkl* expression analysis by qRT–PCR in *Pou2f3*$^{+/+}$ and *Pou2f3*$^{-/-}$ organoids following rIL-4/rIL-13 treatment for 48 h to assess the presence and amplification of tuft cells. Means ± s.d., relative to *Gapdh* and *Hprt*, are presented. **b**, Expansion of the tuft cell lineage in wild-type organoids following rIL-4/rIL-13 administration (48 h) was monitored by Dclk1 staining. **c**, Expansion of the tuft cell lineage in wild-type organoids following IL-4 or IL-13 administration (48 h) was monitored by Dclk1, Pou2f3 and PAS stainings. Scale bars, 20 μm. **d**, *Retnlβ* expression in *Pou2f3*$^{+/+}$ and *Pou2f3*$^{-/-}$ organoids was monitored as a function of rIL-4/rIL-13 treatment (48 h) by RT–PCR and data relative

to *Gapdh* are presented. All panels show representative experiments from 3 independent organoid cultures, replicated 3 times.

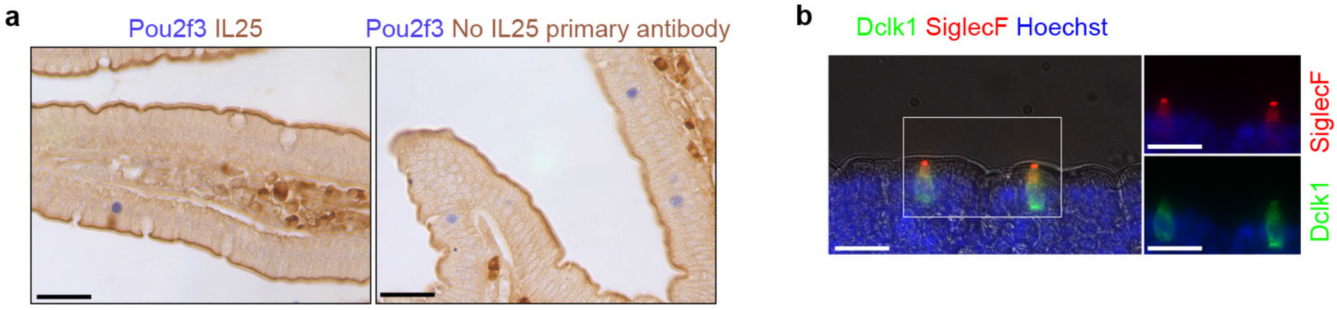

Extended Data Figure 9. Validation of the Siglec-F and IL-25 stainings.

a, Control experiment for specificity of the IL-25 immunohistochemistry, in presence (left) or absence (right) of IL-25 primary antibody. **b**, Immunohistochemistry showing specificity of Siglec-F as a marker for intestinal epithelial tuft cells. All panels show representative experiments from 3 independent mice, replicated 3 times.

Extended Data Table 1
List of the oligonucleotide primer sequences

Primer sets used for qPCR analyses (5’ 3’)

Dclkl	CAGCCTGGACGAGCTGGTGG	TGACCAGTTGGGGTTCACAT
Gapdh	GGAGCGAGACCCCACTAACA	ACATACTCAGCACCGGCCTC
Hprt	GCAGTACAGCCCCAAAATGG	GGTCCTTTTCACCAGCAAGCT

Table 2
Primer sets used for PCR analyses (5’ 3’)

IL13	AG CTCCCTG GTTCTCTCACT	CTCATTAGAAGGGGCCGTGG
IL25	TCTTGGCAATGATCGTGGGA	TGTGGTAAAGTGGGACGGAG
Retnlb	CCAGAAGACCATTTCCTGAGCT	CCCACGATCCACAGCCATAG
Gapdh	CAAGAAGGTGGTGAAGCAGG	TCAAGAGAGTAGGGAGGGCT
Pou2f3	AGAGAATCAACTGCCCCGTG	GGAAGGCACGACTCTCTTCC

Acknowledgements

This work was supported by Association pour la Recherche contre le Cancer (ARC SL220110603456 to P.J.), Agence Nationale de la Recherche (ANR-09-BLAN-0368-01 to P.J., ANR-PolarAttack to V.D. and ANR-14-CE14-0025-01 to P.J. and N.T.), Institut National du Cancer (INCa 2014-174 to P.J.), and the Welcome Trust (Ref. 106122 to RMM). Part of the work was supported by institutional funds of Monell Chemical Senses Center to I.M. E.S. is supported by Ligue Nationale contre le Cancer and NT by Inserm. We are grateful to Marie Pouzolles, Sarah Gaillac and Valérie Zimmermann for their expertise and assistance in immune cell analyses, and to Marc van de Wetering for reagents. We thank Frederic Gallardo and the ZPA facility for maintenance of mouse colonies, the Monell Histology and Cellular Localization Core (supported by funding from NIH Core Grant P30DC011735 (to Robert F. Margolskee, Monell Chemical Senses Center) for some of the histological analyses and Daniel Fisher for critical reading of the manuscript.

References

1. Hotez PJ, et al. Helminth infections: the great neglected tropical diseases. J Clin Invest. 2008; 118: 1311–1321. [PubMed: 18382743]
2. Allen JE, Maizels RM. Diversity and dialogue in immunity to helminths. Nat Rev Immunol. 2011; 11: 375–388. [PubMed: 21610741]
3. Herbert DR, et al. Intestinal epithelial cell secretion of RELM-beta protects against gastrointestinal worm infection. J Exp Med. 2009; 206: 2947–2957. [PubMed: 19995957]
4. McKenzie GJ, Bancroft A, Grencis RK, McKenzie AN. A distinct role for interleukin-13 in Th2-cell-mediated immune responses. Current biology : CB. 1998; 8: 339–342. [PubMed: 9512421]
5. Gerbe F, et al. Distinct ATOH1 and Neurog3 requirements define tuft cells as a new secretory cell type in the intestial epithelium. The Journal of Cell Biology. 2011; 192: 767–780. [PubMed: 21383077]
6. Bezencon C, et al. Murine intestinal cells expressing Trpm5 are mostly brush cells and express markers of neuronal and inflammatory cells. J Comp Neurol. 2008; 509: 514–525. [PubMed: 18537122]
7. Gerbe F, Brulin B, Makrini L, Legraverend C, Jay P. DCAMKL-1 Expression Identifies Tuft Cells Rather Than Stem Cells in the Adult Mouse Intestinal Epithelium. Gastroenterology. 2009; 137: 2179–2180. [PubMed: 19879217]
8. Bjerknes M, et al. Origin of the brush cell lineage in the mouse intestinal epithelium. Developmental Biology. 2012; 362: 194–218. [PubMed: 22185794]
9. Buczacki SJ, et al. Intestinal label-retaining cells are secretory precursors expressing Lgr5. Nature. 2013; 495: 65–69. [PubMed: 23446353]
10. van Es JH, et al. Dll1(+) secretory progenitor cells revert to stem cells upon crypt damage. Nat Cell Biol. 2012; 14: 1099–1104. [PubMed: 23000963]
11. Gierl MS, Karoulias N, Wende H, Strehle M, Birchmeier C. The zinc-finger factor Insm1 (IA-1) is essential for the development of pancreatic beta cells and intestinal endocrine cells. Genes Dev. 2006; 20: 2465–2478. [PubMed: 16951258]
12. Reynolds LA, Filbey KJ, Maizels RM. Immunity to the model intestinal helminth parasite Heligmosomoides polygyrus. Seminars in immunopathology. 2012; 34: 829–846. [PubMed: 23053394]
13. Ishikawa N, Horii Y, Nawa Y. Immune-mediated alteration of the terminal sugars of goblet cell mucins in the small intestine of Nippostrongylus brasiliensis-infected rats. Immunology. 1993; 78: 303–307. [PubMed: 8473019]
14. Watanabe N, Katakura K, Kobayashi A, Okumura K, Ovary Z. Protective immunity and eosinophilia in IgE-deficient SJA/9 mice infected with Nippostrongylus brasiliensis and Trichinella spiralis. Proc Natl Acad Sci U S A. 1988; 85: 4460–4462. [PubMed: 3380800]
15. Matsumoto I, Ohmoto M, Narukawa M, Yoshihara Y, Abe K. Skn-1a (Pou2f3) specifies taste receptor cell lineage. Nat Neurosci. 2011; 14: 685–687. [PubMed: 21572433]
16. Ohmoto M, et al. Pou2f3/Skn-1a is necessary for the generation or differentiation of solitary chemosensory cells in the anterior nasal cavity. Bioscience, biotechnology, and biochemistry. 2013; 77: 2154–2156. [PubMed: 24096675]
17. Yamaguchi T, et al. Skn-1a/Pou2f3 is required for the generation of Trpm5-expressing microvillous cells in the mouse main olfactory epithelium. BMC neuroscience. 2014; 15: 13. [PubMed: 24428937]
18. Bastide P, et al. Sox9 regulates cell proliferation and is required for Paneth cell differentiation in the intestinal epithelium. J Cell Biol. 2007; 178: 635–648. [PubMed: 17698607]
19. Mellitzer G, et al. Loss of enteroendocrine cells in mice alters lipid absorption and glucose homeostasis and impairs postnatal survival. J Clin Invest. 2010; 120: 1708–1721. [PubMed: 20364088]
20. Camberis M, Le Gros G, Urban J Jr. Coligan, John E; , et al. Animal model of Nippostrongylus brasiliensis and Heligmosomoides polygyrus. Current protocols in immunology. 2003.

21. Artis D, et al. RELMbeta/FIZZ2 is a goblet cell-specific immune-effector molecule in the gastrointestinal tract. Proc Natl Acad Sci U S A. 2004; 101: 13596–13600. [PubMed: 15340149]
22. Lawrence RA, Gray CA, Osborne J, Maizels RM. Nippostrongylus brasiliensis: cytokine responses and nematode expulsion in normal and IL-4-deficient mice. Experimental parasitology. 1996; 84: 65–73. [PubMed: 8888733]
23. Urban JF Jr, NobemTrauth N, Schopf L, Madden KB, Finkelman FD. Cutting edge: IL-4 receptor expression by non-bone marrow-derived cells is required to expel gastrointestinal nematode parasites. J Immunol. 2001; 167: 6078–6081. [PubMed: 11714764]
24. Urban JF Jr, et al. IL-13, IL-4Ralpha, and Stat6 are required for the expulsion of the gastrointestinal nematode parasite Nippostrongylus brasiliensis. Immunity. 1998; 8: 255–264. [PubMed: 9492006]
25. Sato T, et al. Single Lgr5 stem cells build crypt-villus structures in vitro without a mesenchymal niche. Nature. 2009; 459: 262–265. [PubMed: 19329995]
26. Moro K, et al. Innate production of T(H)2 cytokines by adipose tissue-associated c-Kit(+)Sca-1(+) lymphoid cells. Nature. 2010; 463: 540–544. [PubMed: 20023630]
27. Neill DR, et al. Nuocytes represent a new innate effector leukocyte that mediates type-2 immunity. Nature. 2010; 464: 1367–1370. [PubMed: 20200518]
28. Zhao A, et al. Critical role of IL-25 in nematode infection-induced alterations in intestinal function. J Immunol. 2010; 185: 6921–6929. [PubMed: 20974983]
29. Barner M, Mohrs M, Brombacher F, Kopf M. Differences between IL-4R alpha-deficient and IL-4-deficient mice reveal a role for IL-13 in the regulation of Th2 responses. Current biology: CB. 1998; 8: 669–672. [PubMed: 9635196]
30. Ohmoto M, Matsumoto I, Yasuoka A, Yoshihara Y, Abe K. Genetic tracing of the gustatory and trigeminal neural pathways originating from T1R3-expressing taste receptor cells and solitary chemoreceptor cells. Mol Cell Neurosci. 2008; 38: 505–517. [PubMed: 18539481]

Europe PMC Funders Author Manuscripts

Europe PMC Funders Author Manuscripts

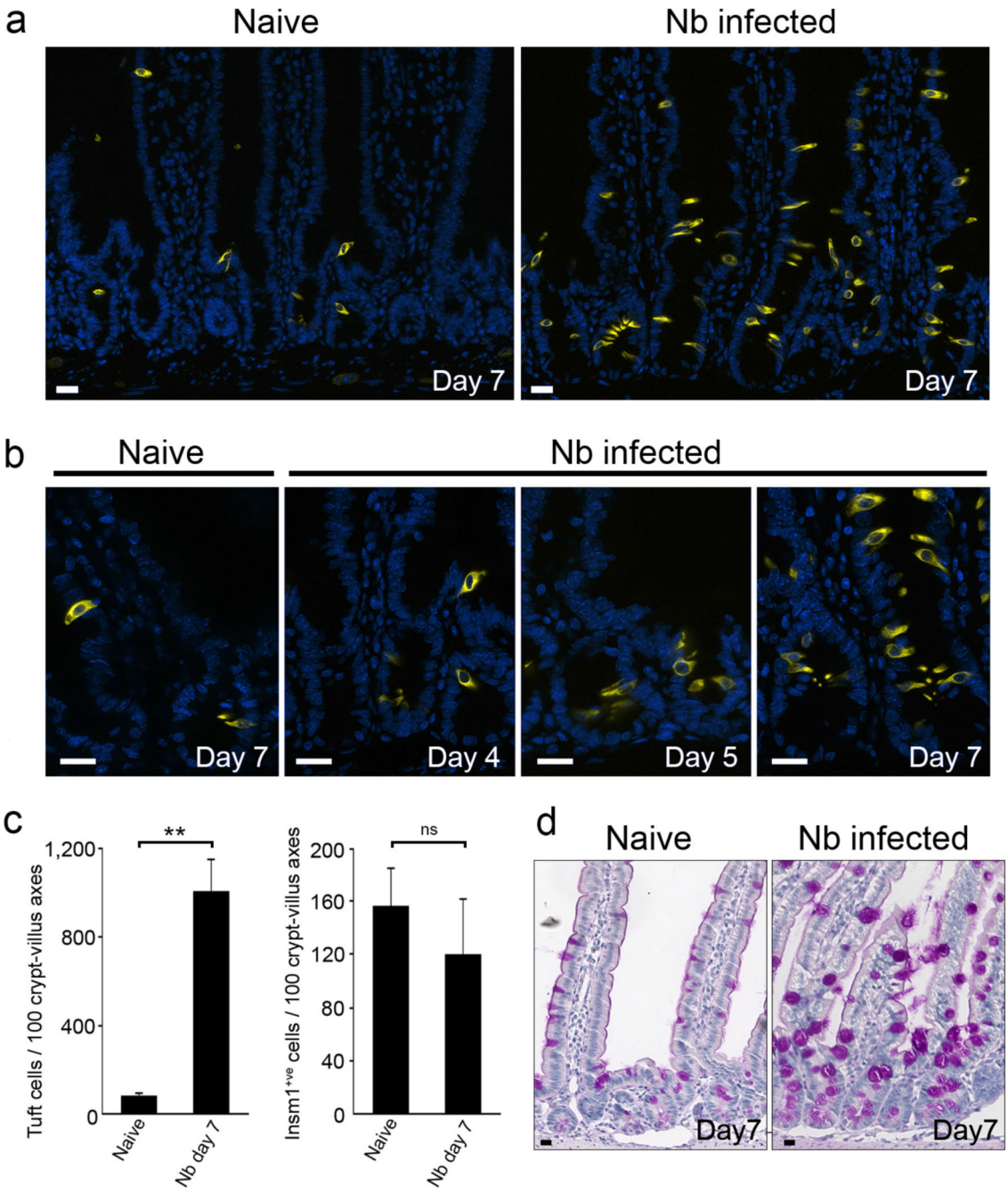

Figure 1. Rapid amplification of the tuft cell lineage following infection with the helminth *N. brasiliensis*.

a : Presence of tuft cells in the intestinal epithelia of naïve and *N. brasiliensis* (*Nb*)-infected mice 7 days post infection, visualized by expression of the Dclk1 marker. b: 8.5 fold increase of tuft cells numbers (1,7±1,4 to 14,4±5,1 per cryptvillus axis) in *Nb*-infected mice as compared to naïve mice, 7 days post infection. Cells were counted in 50 crypt-villus units (n=3 mice per condition). Data are shown as means ± S.D. ($p<0,0001$). c: Changes in the tuft cell population in intestinal crypts are presented at the indicated time points post infection. Quantification is shown in Extended Data Figure 1a. d: Corresponding goblet

cell hyperplasia associated with numerous and larger mucus vacuoles, detected by periodic acid-Schiff (PAS) staining. Dclk1 cells are also visualized in brown. Quantification is shown in Extended Data Figure 1b. For all panels, n=3 mice per condition. Bar: 20μm.

Europe PMC Funders Author Manuscripts

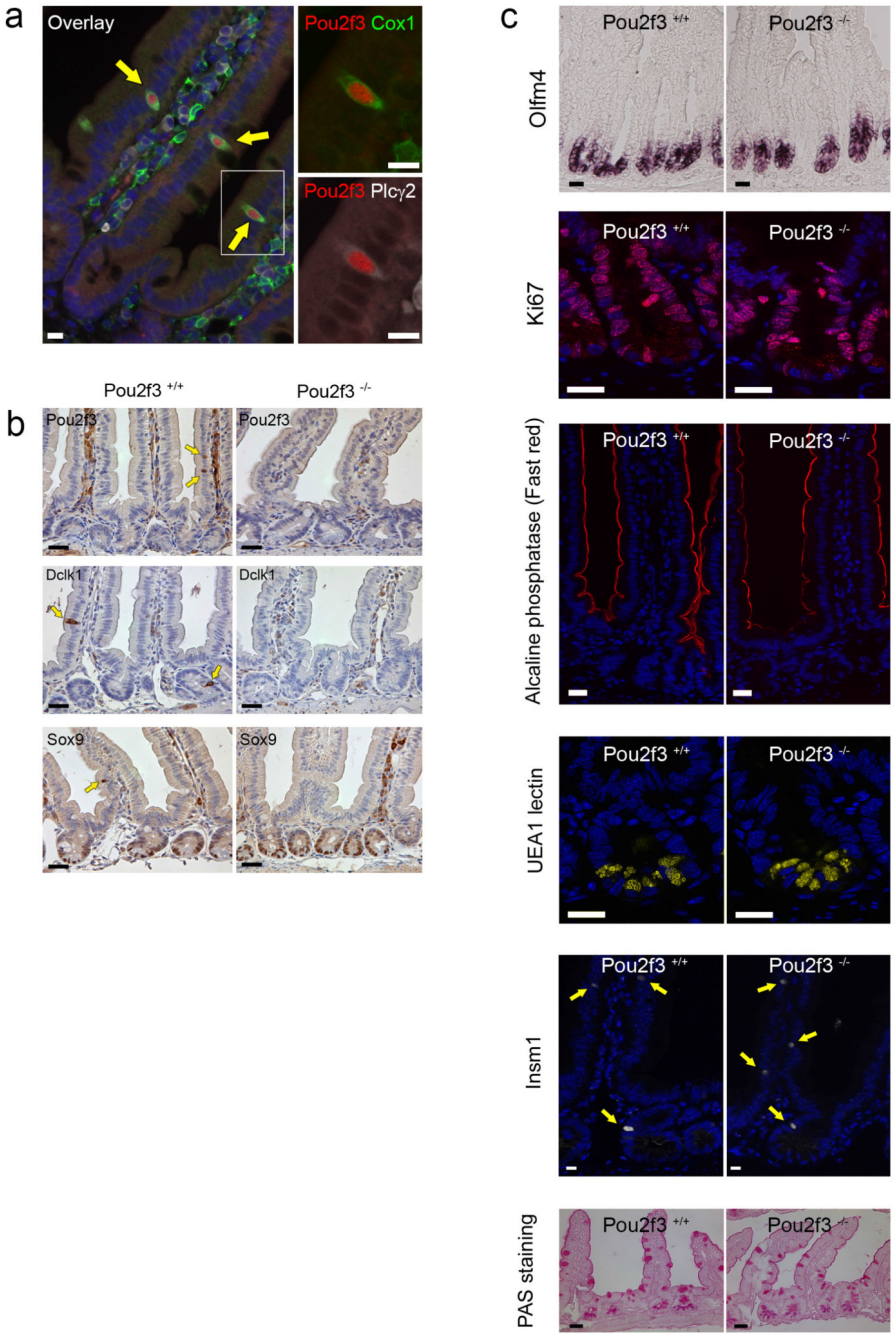

Figure 2. Absence of tuft cells in the intestinal epithelium of Pou2f3 transcription factorEdeficient mice.

a: Pou2f3 is expressed specifically in tuft cells of the intestinal epithelium as determined by co-staining for Pou2f3 and established markers of tuft cells such as Dclk1 and Gfi1b. b: *Pou2f3* deletion results in the absence of tuft cells as monitored by staining intestinal epithelium from *Pou2f3*$^{+/+}$ and *Pou2f3*$^{-/-}$ mice with Pou2f3-, Dclk1- and Sox9-specific antibodies. Bar: 20μm. c. Counting of 50 crypt-villus axes of 3 *Pou2f3*$^{+/+}$ and 3 Pou2f3$^{-/-}$ mice revealed that the *Pou2f3* deficiency does not affect the proliferation zone (p=0,76), stem cell compartment (p=0,53), enterocyte (not counted), goblet (p=0,95), Paneth

(p=0,39) or enteroendocrine (p=0,12) cell lineages as monitored by Ki67, Olfm4, alkaline phosphatase, PAS staining, UEA1 lectin, and Insm1, respectively. Means ± S.D. and p values are indicated. For all panels, n=3 mice per condition.

Europe PMC Funders Author Manuscripts

Europe PMC Funders Author Manuscripts

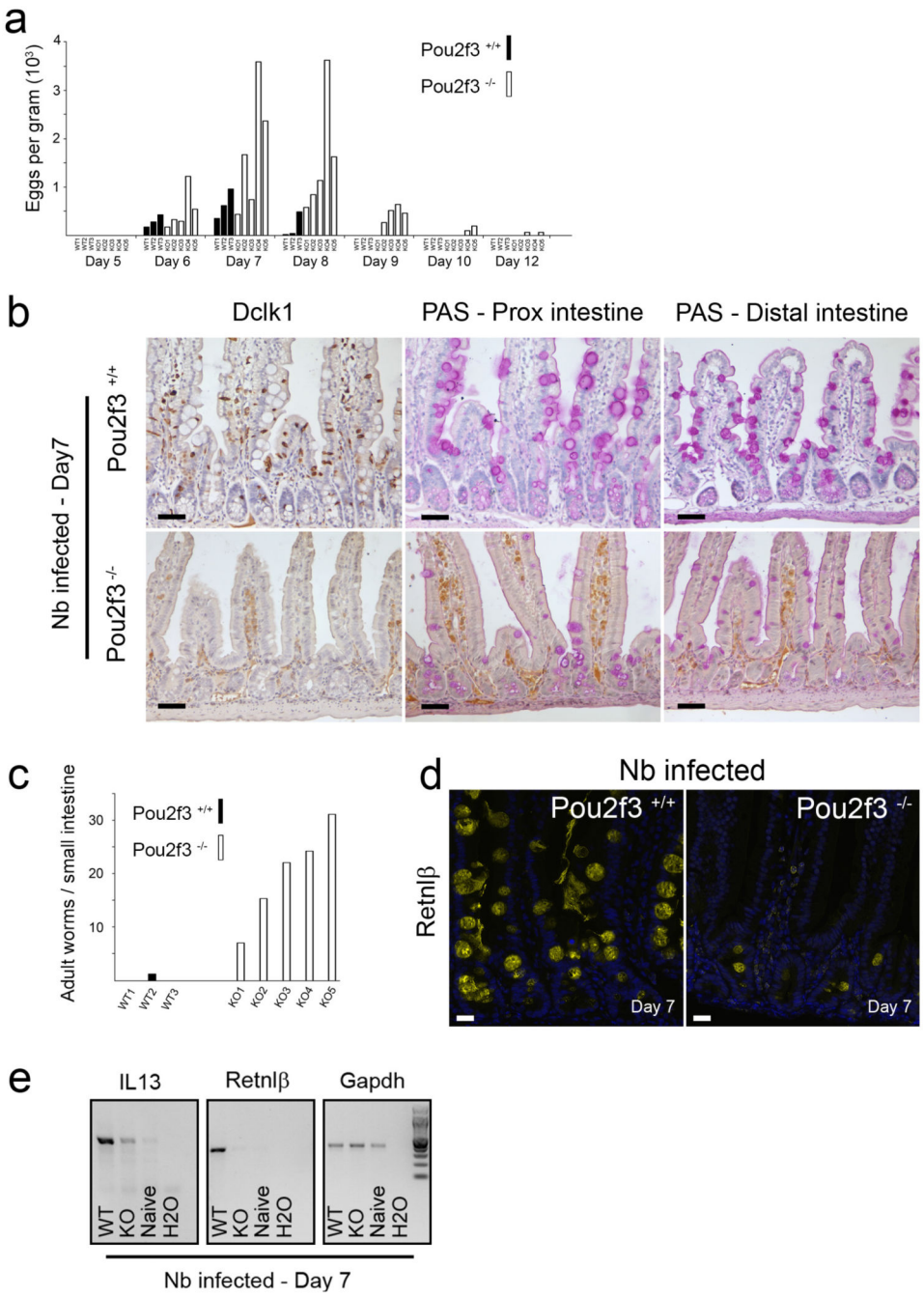

Figure 3. Impaired type 2 responses in *Pou2f3*$^{-/-}$ tuft cell-deficient mice.

a: Live adult worm counts in the small intestines of *Pou2f3*$^{+/+}$ and *Pou2f3*$^{-/-}$ mice at days 9 (left panel) and 13 (right panel) post infection with *N. brasiliensis*. Each bar represents an individual mouse and the WT or KO genotypes are indicated. b: Immunohistochemistry illustrating the proximal and distal small intestinal epithelium of infected *Pou2f3*$^{+/+}$ and *Pou2f3*$^{-/-}$ mice 7 days after infection (3 mice per genotype). Tuft and goblet cells are revealed by Dclk1 and PAS staining, respectively, and the production of Resistin-like beta (Retnlβ) by goblet cells is analysed. Bar: 20μm. c: Quantification of IL13 and Retnlβ in the

intestinal mucosa of naïve, and *Nb*-infected *Pou2f3*$^{+/+}$ and *Pou2f3*$^{-/-}$ mice by RT-PCR, 7 days after infection. Representative gels are shown with relative Gapdh expression presented as an internal control. d: Histological analysis showing tuft (Dclk1 staining) and goblet (PAS staining) cells in naïve and *Nb*-infected *Il4Rα*$^{+/+}$ and *Il4Rα*$^{-/-}$ mice 7 days post infection. For all panels, n>3 mice per condition. Bar: 20μm.

Europe PMC Funders Author Manuscripts

Europe PMC Funders Author Manuscripts

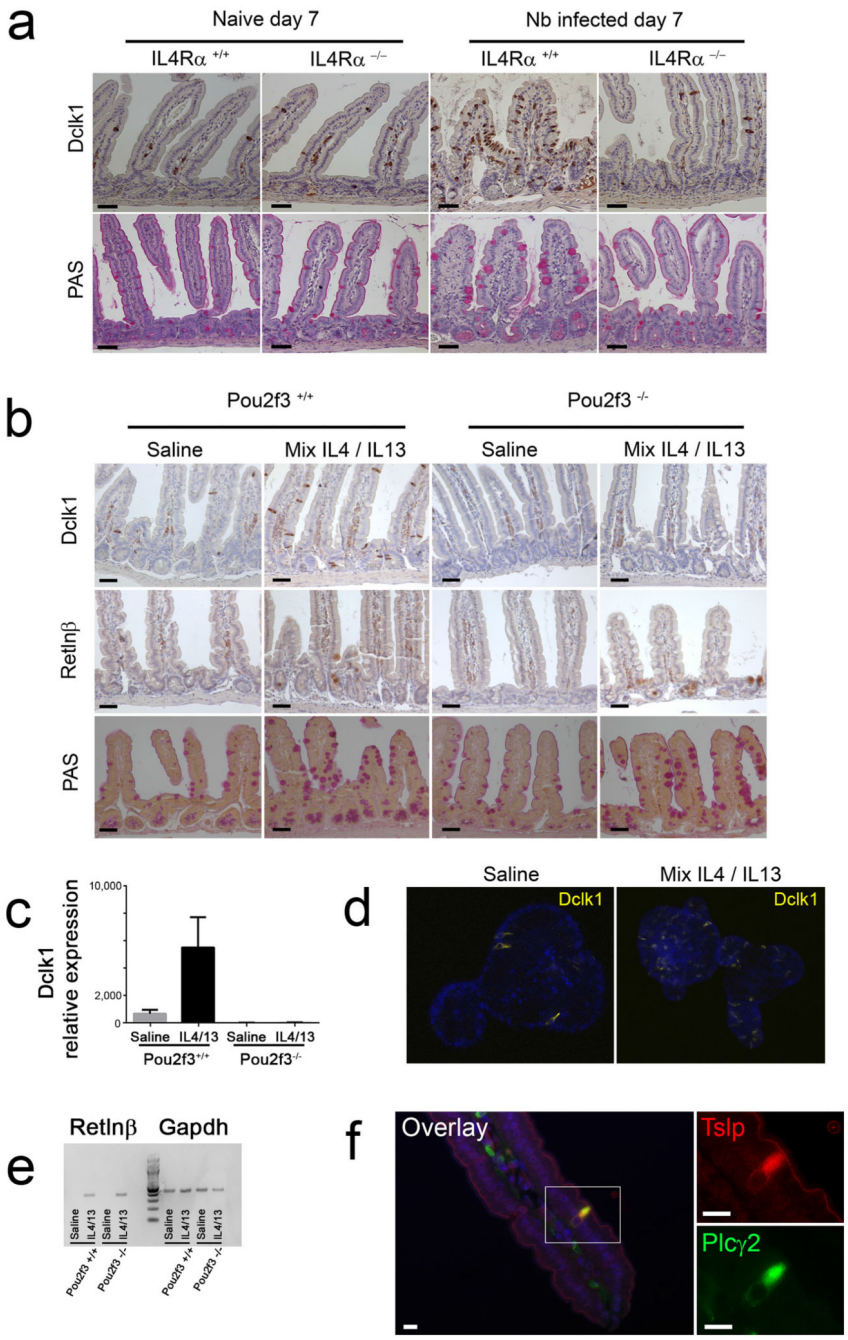

Figure 4. Tuft cells express IL25, and rIL25 is sufficient to initiate type 2 mucosal responses in the absence of tuft cells.

a: Analysis of *Il25* mRNA expression in *Pou2f3*$^{+/+}$ and *Pou2f3*$^{-/-}$ mice infected with *N. brasiliensis*, 9 days posbinfection, by RT-PCR. Data relative to Gapdh are presented. b: Immunohistochemistry showing IL25 expression in naïve and *N. brasiliensis*-infected wild type mice. Blue staining: nuclear Pou2f3 expression revealed with NBT/BCIP. Brown staining: IL25 expression revealed with DAB. n=3 naïve mice and 3 infected mice. Bar: 20μm. c: RT-PCR showing predominant *IL25* and *Pou2f3* mRNA expression in the tuft cells FACS-enriched fractions obtained from 3 independent mice. Gapdh is shown as a control for

loading and RNA integrity. d: Rescue of the *Pou2f3* deficiency by treatment with exogenous rIL25, as assessed by egg counts during a time course of infection with *N. brasiliensis*. N=6 mice per genotype and treatment condition. Means ± S.D. are presented, as well as p values. e: Scheme illustrating the function of tuft cells in initiating type 2 responses following infection with intestinal helminths. Left part: normal epithelium undergoing infection with an helminth. Right part: tuft cell-dependent epithelial remodelling during type 2 responses.

Europe PMC Funders Author Manuscripts